Journal of Photochemistry and Photobiology A: Chemistry 200 (2008) 254–261

Contents lists available at ScienceDirect

Journal of Photochemistry and Photobiology A: Chemistry

journal homepage: www.elsevier.com/locate/jphotochem

Photocatalytic degradation of ammonia and butyric acid in plug-flow reactor: Degradation kinetic modeling with contribution of mass transfer

Benoit Boulinguiez[a], Abdelkrim Bouzaza[a,*], Smail Merabet[b], Dominique Wolbert[a]

[a] Laboratoire Sciences Chimiques de Rennes - Équipe Chimie et Ingénierie des Procédés, UMR 6226 CNRS, ENSCR, Avenue du Général Leclerc, 35700 Rennes, France
[b] Laboratoire d'hydraulique Appliquée et Environnement, Université de Béjaïa, Route de Targa Ouzemour, Bejaïa, Algeria

ARTICLE INFO

Article history:
Received 14 March 2008
Received in revised form 18 July 2008
Accepted 2 August 2008
Available online 22 August 2008

Keywords:
Photocatalysis
Kinetic modeling
Ammonia
Butyric acid
Mass transfer
Annular reactor
Langmuir–Hinshelwood

ABSTRACT

Photocatalytic treatment of polluted air by odorous contaminants – ammonia and butyric acid – is investigated in a plug-flow reactor covered by non-woven fiber textile coated with TiO_2. For the first time, the single-component degradation pathway of ammonia by photocatalysis at ambient condition is highlighted. It appears fundamentally different compared to the butyric acid degradation pathway. The ammonia degradation pathway highlights a possible auto-accelerated behavior of the reaction. The chemical degradation kinetics follows the Langmuir–Hinshelwood model, though observed oxidation rates depend upon flow conditions in the reactor. Thus, interpretation of degradation results through a model considering the Langmuir–Hinshelwood approach and mass transfer phenomenon is presented. This model succeeds with a pair of determined kinetic constants and mass transfer coefficients to describe experimental results for different flow rates and for both pollutants, though they present wide dissimilarities in their degradation pathways.

1. Introduction

Air pollution has become major public concern for few decades. Industrials from all sectors have seen their gas rejections controlled and limited for environmental considerations [1]. Each International protocol since 1979 has fixed new regulation and has gradually reduced rejection limit of major pollutants. The need of efficient, easy-to-apply and sure process is exponential. Existing processes for air treatment such as incineration, absorption, adsorption, condensation and biofiltration have their own application fields and limits [2]. The demand for a compact simple system that could carry out complete destruction at moderate conditions of various oxidizing compounds is obvious. As a matter of fact photocatalytic treatments arise among promising solutions for air depollution [3,4].

The photocatalysis, which belongs to advanced oxidation process (AOP) family, needs a wide bandgap semiconductor stimulated by light irradiation combined with the presence of an oxidizer such as oxygen for air treatment. TiO_2 is generally believed to be a potentially efficient catalyst in photocatalytic treatments [5]. Moreover it presents few essential qualities for industrial interest: abundance, stable performance, durability and low production cost. As a consequence, the majority of photocatalytic research efforts utilize TiO_2 as catalyst, despite the necessity to activate it by UV radiation [6,7].

Photocatalysis or photocatalytic oxidation (PCO) could possibly oxidize pollutants into innocuous products such as CO_2 and H_2O [8]. The photoreactions involved at the surface of the irradiated catalyst produce reactive species like HO^o which is considered as the primary oxidant in presence of water. Production rate and stability of radicals are controlled by relative humidity, UV intensity, product and by-product chemical characteristics [7,9,10].

Photocatalytic systems have been regularly studied through volatile organic compounds (VOC) degradation due to their considerable occurrence in industrial domains and air pollution [11–14].

Three main steps interfere in the apparent degradation rate of a pollutant: (i) the mass transfer (MT) of the pollutant from the bulk phase to the photocatalysis surface, (ii) the adsorption of the pollutant on the photocatalytic medium, (iii) the surface reaction.

Abbreviations: r, average degradation rate (mmol m^{-2} s^{-1}); in/out, exponent denomination for inlet and outlet; Q, volumetric flow rate (m^3 s^{-1}); S, catalytic medium surface (m^2); k, degradation rate constant (mmol m^{-3} s^{-1}); K, equilibrium adsorption constant (m^3 $mmol^{-1}$); Re, Reynolds number; Sh, Sherwood number; Sc, Schmidt number; r', rate of reaction per unit of catalyst (mmol m^{-3} s^{-1}); d_L, characteristic dimension of the deposit (m); k_m, mass transfer coefficient (m s^{-1}); d_{eq}, equivalent diameter for the annular reactor (m); L, length of the reactor covered by the medium (m); L_{tot}, length between the inlet and outlet of the reactor (m); D, diffusivity in the air (m^2 s^{-1}); a_v, effective catalyst area per unit volume of reactor (m^2 m^{-3}); C, bulk gas-phase concentration (mmol m^{-3}); C^*, medium surface gas-phase concentration (mmol m^{-3}).

* Corresponding author. Tel.: +33 2 23238056; fax: +33 2 23238120.
E-mail address: abdelkrim.bouzaza@ensc-rennes.fr (A. Bouzaza).

1010-6030/$ – see front matter © 2008 Elsevier B.V. All rights reserved.
doi:10.1016/j.jphotochem.2008.08.005

The desorption and diffusion steps of the product and by-products are usually negligible.

The pollutant mass transfer is dependant on the catalyst configuration, reactor geometry, pollutant concentration and aerodynamic conditions in the reactor [11,15,16]. In most cases, steady-state kinetic models in the literature ignore the influence of mass transfer. That could be presumed if turbulences in the system are high enough to consider the surface reaction as the limiting step in the apparent degradation rate [9,17]. Thus, the pollutant adsorption and the oxidative reaction are usually described by the Langmuir–Hinshelwood theory [3,5,6].

When mass transfer has not been occulted, authors have developed kinetic models by considering a first-order kinetic though it can only be applied at low compound concentrations [18,19]. At higher concentrations zero-order kinetics are observed. A promising approach of a global model taking into account the mass transfer and the photocatalytic reaction – based on the Langmuir–Hinshelwood theory – has been reported recently [20].

Our study is conducted in an annular plug-flow reactor in thin film configuration where butyric acid (a VOC) and ammonia are the tested pollutants. That technique has barely investigated ammonia as pollutant in spite of its wide presence as a reactant or product in various activities [21–23]. For instance, this couple of pollutants presents a high occurrence in agricultural industries [24–26].

The global purpose is to determine whether the kinetic degradation of both pollutants can be studied in the same reactor and correlated by the same general model where mass transfer is not neglected despite likely dissimilarities in their reaction pathways. To investigate the effect of pollutant concentration and flow rate on the apparent degradation rate, other parameters are kept constant: temperature, relative humidity (RH), oxygen concentration and UV irradiation.

2. Experimental

2.1. Apparatus

Fig. 1 represents the used apparatus. A regulated centrifugal pump generates, from the ambient air, a flow rate controlled by a flow meter (Bronkhorst IN-FLOW). The stream is partially deviated through a packed column working in countercurrent with water. Resulted RH is $50 \pm 3\%$ at $30 \pm 3\ ^{\circ}C$. Then, the synthetic air effluent is prepared. Ammonia is supplied from a cylinder containing 3% molar ammonia in nitrogen, the flow rate of which is controlled by the AALBORG GFC17 analogue flow meter coupled to an accurate valve. For experiments carried out with butyric acid, a syringe/syringe driver system injects the liquid pollutant through a septum into the gas stream. A heating system covering the injection zone sets the gas temperature and facilitates the butyric acid vaporization ahead of the static mixer.

It should be noted that whether the UV lamp could potentially heat up the air; the outlet temperature of the gas never exceeds the above-mentioned value. It has been confirmed by experimental outlet temperature measurements. This is due to the open continuous reactor where the air-flow evacuates the heat.

The effluent is sent in the annular photoreactor (Fig. 2) between two concentric cylinders (Ø58 and 76 mm). The inner surface of the large cylinder is covered with the photocatalytic medium. That reactor part develops 0.19 m^2 surface over 80 cm in length. Thus the effective medium surface per unit volume of the reactor is 126 $m^2\ m^{-3}$. Two sampling points, sealed off with septum are used to analyze the inlet and outlet gas composition of the photoreactor. The outlet flow is partially oriented through a scrubbing system for ammonia analysis (see Section 3).

The light source used in this study is a 1.5-m long, 80 W UV lamp with a major wavelength peak emission at 360 nm (Philips CLEO performance). The light tube is placed in the inner concentric cylinder. Light intensity measured at the medium surface is $30 \pm 2\ W\ m^{-2}$ at 365 nm.

2.2. Photocatalytic medium

The medium provided by Alhström is a perforated non-woven textile composed of cellulosic fibers coated with a mix of catalyst (TiO_2 Millénium PC 500, specific area = 317 $m^2\ g^{-1}$), zeolite and silica. Their mass per square meter is respectively 16.5, 3.4 and 13.3 $g\ m^{-2}$. The support is 250 μm thick. The median diameter of deposited pellets on the medium is 1.4 μm.

2.3. Experimental procedure

Preliminary step is the air stream conditioning: temperature, flow rate and humidity. Then the pollutant is injected continuously at specific rate to reach the desired inlet concentration. The reactor is loaded 120 min with the light off so as to overpass the transient phase. During that period air constituents (water, pollutant) are adsorbed on the medium surface. Equilibrium between the solid phase and the gas phase is achieved when the inlet concentration and the outlet concentration become equal. The lamp is then turned on creating a second transient period that precedes the steady-state

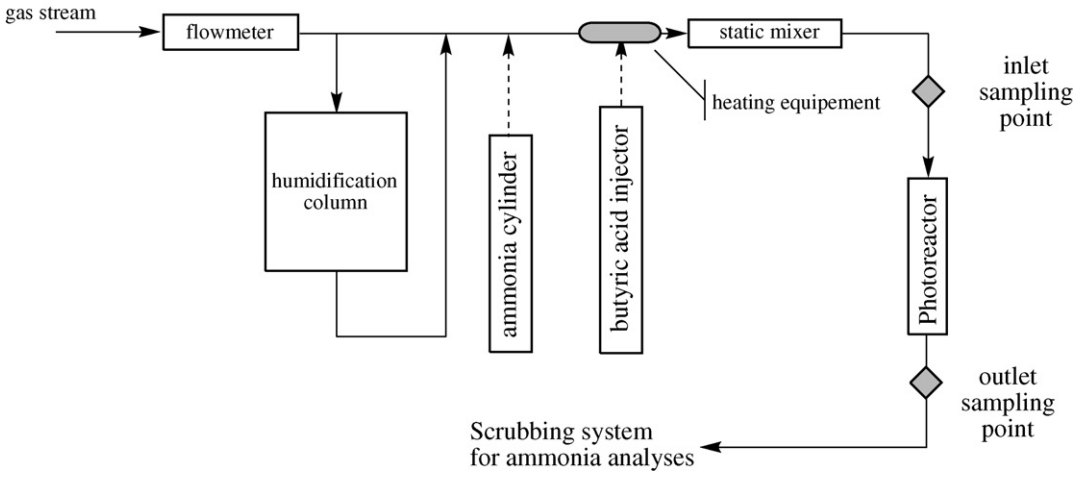

Fig. 1. Experimental setup.

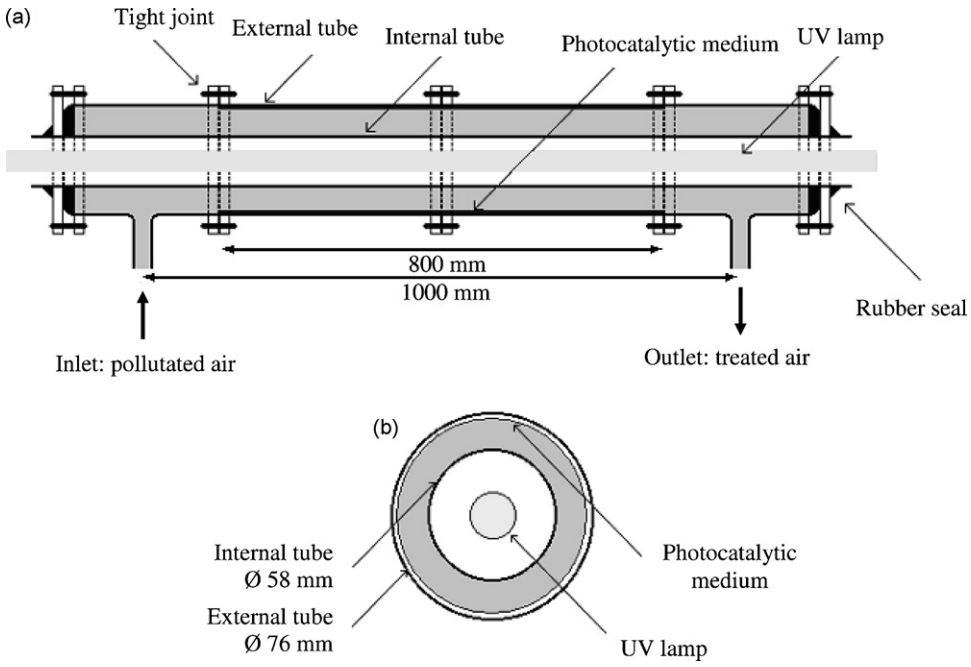

Fig. 2. Scheme (a) and sectional drawing (b) of the annular photoreactor.

stage when the pollutant concentration in the outlet remains time relative constant.

Each pollutant is the root of a three-different flow rate test 2, 4 and 6 $m^3\,h^{-1}$ in a defined pollutant concentration range.

3. Analysis

Butyric acid samples are taken using 500 or 1000 μL chromatographic syringe and then immediately injected into a gas chromatograph (Fisons GC 9000 series) equipped with a capillary column (Chrompact FFAP-CB) dedicated to the separation of volatile fatty acids (VFA). Nitrogen is used as gas carrier to a flame ionization detector. Analysis conditions are as follows (Table 1).

The ammonia trapped in the scrubbing system is quantified by molecular absorption spectrophotometric method. The Nessler reagent is employed to obtain colored solutions by reaction 1:

$$\underset{}{NH_4^+} + 2\underset{\text{Yellow}}{[HgI_4]^{2-}} + 4HO^- \rightarrow HgO \cdot \underset{\text{Brown}}{Hg(NH_2)I} + 7I^- + 3H_2O \qquad (1)$$

4. Results and discussion

Photocatalytic treatments present major interests for air depollution. However, more thorough study of new systems is necessary to evaluate potential risk of such technology. One part of that approach is to understand and, if possible, forecast the degradation of pollutant to predict the by-product formation.

4.1. Degradation path of pollutants

4.1.1. Butyric acid—$C_4H_8O_2$

The photocatalytic oxidation scheme of VFAs consists of the simultaneous carboxylic function removal and alcoholic function creation [27–29]. That new function is immediately oxidized in a ketone initiating a new carboxylic function carried on a '$n-1$' carbon molecule. A degradation pathway has been proposed from literature study and has been checked through experimental investigations [14,30].

That degradation pathway in series leads to a complete mineralization of the pollutant as represented in Fig. 3.

In our experimental conditions, the complete mineralization is not obtained [20,30]. Thus, the presence of intermediates may influence the degradation rate of butyric acid through competitive adsorption. Prior study has shown that concentrations of intermediates (alcohols and ketones) are low compared to the butyric acid one and acids are stronger adsorbed on the media than their intermediates [30]. Therefore the by-products are partially purged in the air stream [14]. Hence, influence of subsequent reaction intermediates is not considered in the degradation rate of butyric acid.

4.1.2. Ammonia—NH_3

VFA behaviour in photocatalytic oxidation is clearer than the ammonia one. First studies concerning ammonia photocatalytic oxidation mentioned, among by-products, the existence of nitrogen and nitrous oxide. The advanced kinetic model laid on a non-determined by-product, hypothetically HNO and did not involved radicals [21]. Few years later, the study of nitric oxide/ammonia photocatalytic degradation has pointed out the role of adsorbed NH_2NO on the media as a reaction intermediary, thus it has validated a conclusion emitted by Mozzanega et al. [21]. Furthermore, the advanced mechanism justifies the formation of nitrogen and water during the degradation [31,32]. The mechanism is described in Fig. 4:

The nitric oxide/ammonia couple photocatalytic degradation has been additionally studied in oxygen free atmosphere. Isotopic

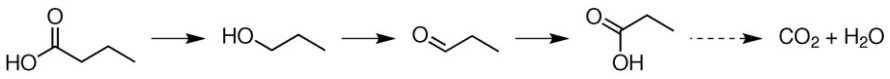

Fig. 3. Degradation scheme of volatile fatty acids by photocatalysis.

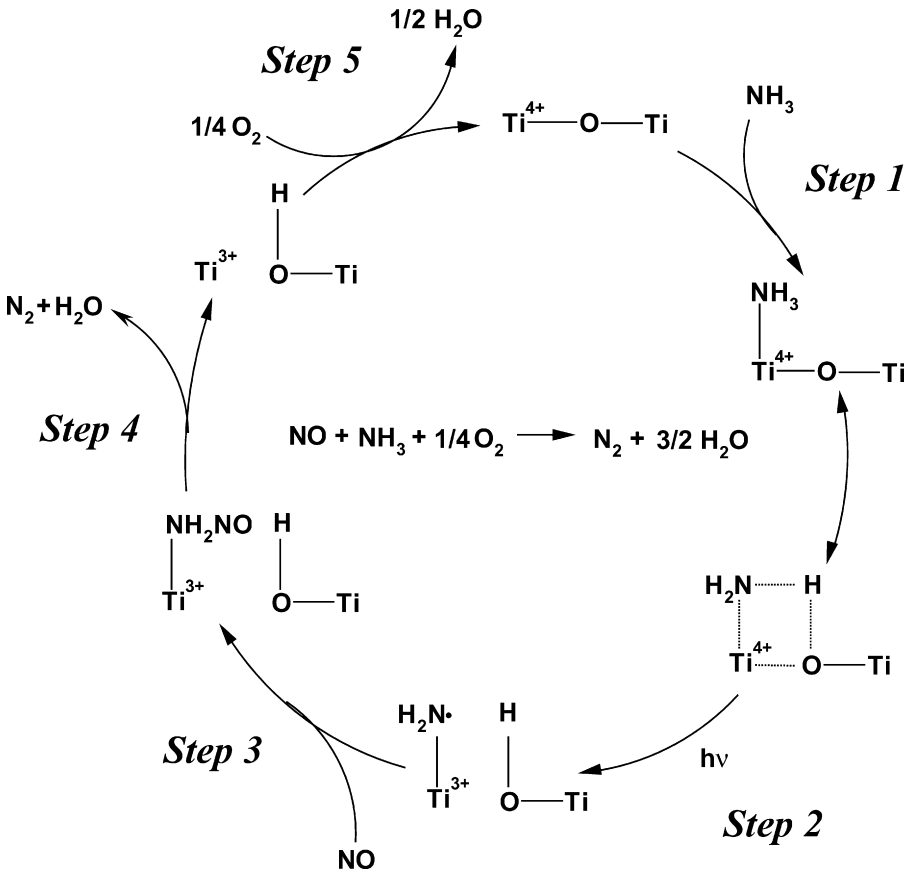

Fig. 4. Degradation scheme of the couple nitric oxide/ammonia by photocatalysis by Teramura et al. [31].

investigations confirm that produced nitrogen comes from the reaction between nitric oxide and ammonia whereas nitrous oxide is exclusively formed from nitric oxide [33].

The formation of nitrogen dioxide from nitric oxide by photocatalytic oxidation has been widely studied by works on NO_x for urban atmospheric depollution. The reaction pathways are detailed as follows [34]:

$$NO + HO^{o} \rightarrow HNO_2 \quad (2)$$

$$HNO_2 + HO^{o} \rightarrow NO_2 + H_2O \quad (3)$$

The by-products evoked by Mozzanega et al. are all confirmed through these studies. However, these studies neither investigate the photocatalytic single-component degradation of ammonia nor the degradation in ambient temperature and oxygen concentration conditions.

By-products formation during ammonia photooxidation in ambient conditions has been experimentally inspected [23,24,35]. Yamazoe et al. [22] pointed out that the adsorbed ammonia on the Lewis acid sites of TiO_2 reacts with the different oxygen radicals to form nitric oxide which is oxidized to give nitrogen oxides. They concluded as well that nitrogen dioxide is more active than other surface nitrogen oxides species, and react with adsorbed ammonia to form NH_2NO_x species decomposed in N_2. These aspects have been observed in the study [30,35] as well: nitrogen gas is the major product of ammonia degradation; nitric oxide is a valuable intermediary for the ammonia degradation; nitrous oxide is produced from nitric oxide at low rate.

Combining experimental results and the various hypotheses from presented papers, the following degradation pathway is considered for ammonia photocatalysis (Fig. 5).

To recapitulate, both pollutants exhibit fundamental dissimilarities in their chemical properties and degradation pathway. Butyric acid belongs to the organic acid group and ammonia is considered as a mineral base. Butyric acid follows linear decarboxylation whereas ammonia presents apparently auto acceleration in its degradation pathway. Such pollutant investigations may be worthy if dissimilarities are observed among photodegradation performances.

4.2. Results interpretation

In Fig. 6, the variation of the oxidation rate of butyric acid and ammonia are represented as a function of the inlet concentration for different effluent flow rates. The average oxidation rate r is calculated by Eq. (4).

$$r = \frac{(C^{in} - C^{out}) \times Q}{S} \quad (4)$$

where C^{in} and C^{out} are respectively the inlet and outlet pollutant concentration, Q is the volumetric flow rate and S the medium surface.

Both pollutants behave similarly with the variation of chosen parameters (flow rate and inlet concentration of contaminant),

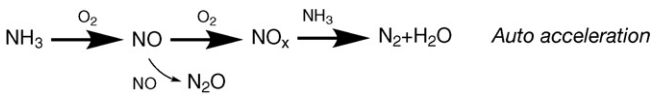

Fig. 5. Degradation scheme of ammonia by photocatalysis (the bold arrow defines the main degradation pathway under atmosphere with oxygen).

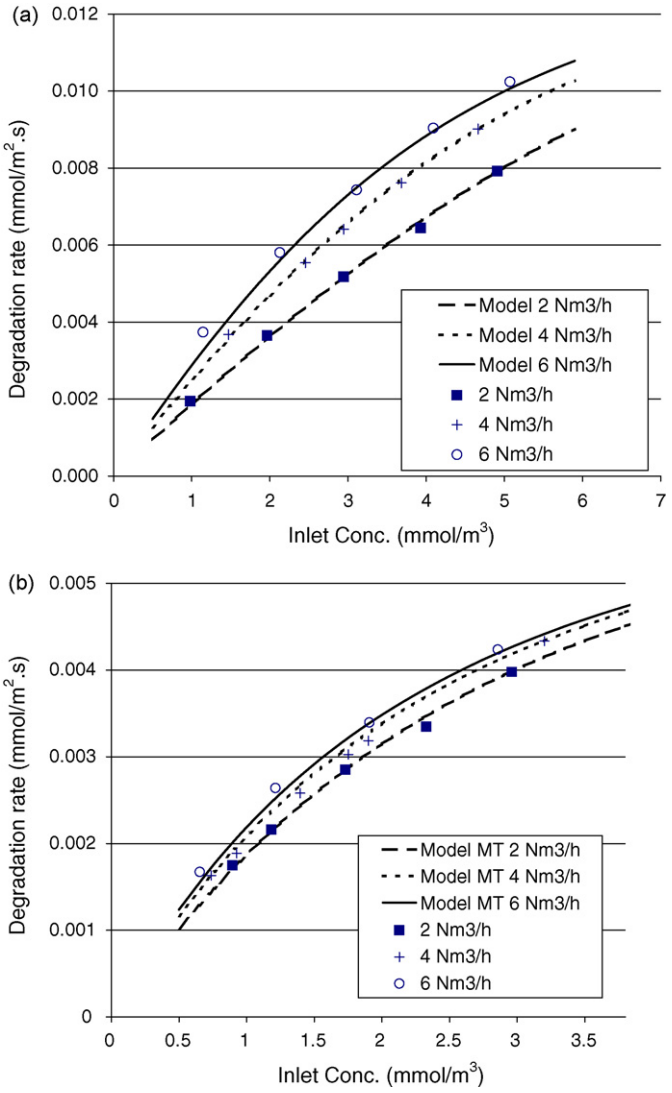

Fig. 6. Degradation rate vs. the inlet concentration of butyric acid (a) and ammonia (b) for the investigated flow rates.

though they present a different reaction way for their mineralization.

For a selected flow rate, the degradation rate increases with the inlet concentration. For diluted effluent, the oxidation rate is directly proportional to the inlet concentration. The degradation occurs to fit a first-order kinetic. In this specific concentration range, many photoactive sites remain available for the reaction. At higher pollutant concentration, the rate tends to a limit explained by the increase of occupied sites. According to the L–H theory, any further increase of the inlet concentration will not result to a proportional increase of the degradation rate. This phenomenon is confirmed by the curve shape at highest concentrations.

Results in Fig. 6 show that the apparent oxidation rate of pollutants increases with increasing flow rate. In laminar regime, the flow rate increase involves higher values of the Reynolds number (Re) from 368 to 1103 and mass transfer coefficient (k_m) [15]. The gas-phase mass transfer rate influences the treatment capacity by producing a concentration gradient between the bulk and the medium surface. However that assumption could not be extended to all regimes, for instance under transitional conditions, the apparent oxidation rate depends on gas-phase mass transfer rate and surface reaction rate [36]. At higher flow rate the process becomes chemical step controlled.

4.2.1. Results interpretation by the model without mass transfer (wMT)

In that first part, the kinetic model arises from the surface reaction step considerations. The degradation rate is apparently first order at low concentration and zero order at higher values. Respecting the previous observations, kinetics of single-component in heterogeneous photocatalytic treatments often follow the Langmuir–Hinshelwood model [17,37–39].

$$r = k\frac{KC}{1+KC} \tag{4}$$

where r is the degradation rate, K is the adsorption constant, k is the kinetic constant and C is the contaminant bulk concentration. In such a model, the adsorption and desorption stages are kinetically negligible in comparison with the oxidizing reaction step; the adsorption rate of the pollutant is higher than any by-products adsorption rate and binding products do neither interact with each other nor modify the initial activity of reactive sites. In batch reactor k and K values can be deduced directly from the linear form of the Eq. (4). In the continuous plug-flow reactor the overall mass balances on the different phases are required [18,40]. The reactor has been confirmed as a plug-flow reactor [30]. To do this, a residence time distribution (RTD) experiment was carried out using carbon dioxide as a tracer substance. This last was injected during a very short time interval into the reactor (Dirac function). The outlet carbon dioxide concentration is measured using an infrared detector (Cosma Beryl). The tanks in series model was used to describe the response of the system. The experiments of RTD revealed that our annular reactor could be assimilated to a cascade of 22 elementary continuously stirred tank reactors. It is generally accepted that above a number of 20 elementary reactors, the experimental reactor can be considered as a plug flow reactor [41].

In the plug-flow reactor at the steady state, the continuous pollutant degradation along the axial direction should not be ignored. The continuity equation for a contaminant is

$$u\frac{dC}{dz} = -r \Rightarrow u\frac{dC}{dz} + k\frac{KC}{1+KC} = 0 \tag{5}$$

Eq. (5) is then integrated for z and C along the photoreactor length coated by the medium to give

$$-u\int_{in}^{out}\frac{1+KC}{kKC} = \int_0^L dz \tag{6}$$

After integration and linear rearrangement Eq. (7) is obtained:

$$\frac{\ln(C^{out}/C^{in})}{C^{out}-C^{in}} = \frac{kKL}{u}\frac{1}{C^{in}-C^{out}} - K \tag{7}$$

where L is the reactor length covered by the medium, u is the superficial gas velocity and z is the axial direction of the reactor. The coefficients k and K are determined by fitting results for each flow rate and contaminant with the linear Eq. (7) (Table 2 and Fig. 7). The confidence interval of each parameter is determined with a confidence level $(1-\alpha)$ of 95%. The cross-correlation coefficient is defined as the covariance of the couple k and K divided by each parameter standard deviation σ_k and σ_K.

Despite high R^2, the coefficients are flow rate dependent for both products. The confidence intervals of the parameter are small but the cross-correlation coefficient clearly indicates that the parameter assessment is significantly linked. This is due to the linear transformation of the model which exhibits direct determination of K with the intercept but indirect determination of k from K with the

Table 1
Analysis conditions for the gas chromatograph

Gas pressure			Zone temperature		
N_2 (gas carrier, kPa)	H_2 (kPa)	Air (kPa)	Injector (°C)	Oven (°C)	FID (°C)
105	40	100	200	115	250

Table 2
Values of the kinetic coefficients determined with the model wMT

	Butyric acid			Ammonia		
	2 $Nm^3 h^{-1}$	4 $Nm^3 h^{-1}$	6 $Nm^3 h^{-1}$	2 $Nm^3 h^{-1}$	4 $Nm^3 h^{-1}$	6 $Nm^3 h^{-1}$
k (mmol $m^{-3} s^{-1}$)	2.72 ± 0.05	2.81 ± 0.08	2.21 ± 0.13	0.84 ± 0.04	0.95 ± 0.04	0.92 ± 0.04
K (m^3 $mmol^{-1}$)	0.15 ± 0.02	0.17 ± 0.02	0.28 ± 0.05	0.62 ± 0.08	0.45 ± 0.06	0.55 ± 0.07
R^2 (%)	99.93	99.97	99.69	99.81	99.67	99.96
Cross-correlation	0.874	0.950	0.932	0.957	0.950	0.940

slope coefficient kKL/u. The model wMT shows its limits in our conditions, though the linearity of the fitting model is observed on the experimental values [39]. The mass transfer contribution is intrinsically included in the determined k and K which can be therefore considered as apparent constants. More realistic values of k and K factors can be approached either with tests at higher flow rate, when the surface reaction is kinetically step determinant, or with a model containing explicit mass transfer coefficients related to the reactor design.

4.2.2. Results interpretation by the model taking into account MT

In photooxidation process with immobilized catalyst, internal and external mass transfer ought to be considered. The relationship of the observed degradation rate, the external and internal mass transfer rates and the intrinsic kinetic reaction rate is comparable to the expression of resistance in series, as follows [16]:

$$\frac{1}{k_{obs}} = \frac{1}{k_{rea}} + \frac{1}{k_{int,TM}} + \frac{1}{k_{ext,TM}} \quad (8)$$

The external mass-transfer resistance is due to the convection of the pollutant molecule from the bulk phase to the catalyst surface. It can be reduced by increasing the circulation flow rate.

The diffusion phenomenon of organic molecules within porous catalyst media defines the internal mass transfer resistance. It is an intrinsic property of the catalyst film and determined by the nature of the catalyst and the coating techniques used. It can be evaluated using the non-dimensional Weisz–Prater modulus φ'. The latter is a derived form of the Thiele modulus [42]. The Weisz–Prater modulus is based on observable parameters; its expression is as follows:

$$\varphi' = \frac{r' d_L^2}{D_e C^*} \quad (9)$$

where r' is the experimental rate of reaction per unit of catalyst, d_L the characteristic dimension of the deposit, C^* the medium surface gas-phase concentration and D_e is the effective diffusivity. Effective diffusivity is defined as

$$D_e = \frac{D\varepsilon}{\tau} \quad (10)$$

where D is the diffusion coefficient of the pollutant, ε is the porosity of the catalyst and τ the tortuosity of the catalyst. The porosity and tortuosity are respectively equal to 0.5 and $\sqrt{3}$ [20]. The medium surface gas-phase concentration, C^* has to be known in order to calculate the Weisz–Prater modulus. It is possible to evaluate the medium surface gas-phase concentration, C^*, in function of the bulk concentration by the Eq. (12). Thus, the Weisz–Prater modulus can be calculated.

For butyric acid, it has been shown that there is no limitation by internal mass transfer [20]. For ammonia let us calculate the value of the Weisz–Prater modulus in the worst conditions which are 2 $Nm^3 h^{-1}$ flow rate at the lowest concentration (C = 0.80 mmol m^{-3}, C^* = 0.32 mmol m^{-3}). The calculated Weisz–Prater modulus is estimated about 7×10^{-6}. It is assumed that an internal mass transfer limitation occurs when $\varphi' > 1$. Therefore, the internal mass transfer step limitation is not considered in our condition. It should be noted that photocatalysis implies superficial reaction sites; therefore it seems coherent that internal diffusions, either Knudsen or Molecular, are negligible.

Hence, there is no internal mass transfer limitation for ammonia as well and the model MT considers only the effect of external mass transfer in the apparent degradation rate for the Eqs. (11) and (12).

According to the film diffusion model, the overall mass balance, on the photoreactor becomes

$$\text{Gas phase}: \quad u\frac{\partial C}{\partial z} + k_m a_v (C - C^*) = 0 \quad (11)$$

$$\text{Solid phase}: \quad k_m a_v (C - C^*) - k\frac{KC^*}{1 + KC^*} = 0 \quad (12)$$

where C and C^* are respectively the bulk and the medium surface gas-phase concentrations of the substance, k_m is the mass transfer coefficient and a_v is the medium area per unit volume of the reactor.

The mass transfer term k_m is estimated by semi empirical expression for laminar flows in annular reactor [14].

$$Sh = 1.029 \times Sc^{0,33} \times Re^{0.55} \times \left(\frac{L_{tot}}{d_{eq}}\right)^{-0.472} \quad (13)$$

where Sh, Sc and Re are respectively Sherwood, Schmidt and Reynolds numbers. Pollutants diffusivities are calculated by the Fuller, Schettler and Giddings correlation [43]. Key values are summarized in Table 3.

Once mass transfer coefficients are calculated, it is generally agreed that the kinetic is a first-order type so as to consider $KC^* < 1$ in order to simplify Eqs. (11) and (12) into a linear integrative system [38]. However, it has been shown that the software Maple could

Table 3
Values for the diffusivity, the Reynolds number and the mass transfer coefficients in the annular reactor

	Butyric acid	Ammonia
Diffusivity in the air (D, $cm^2 s^{-1}$)	0.0897	0.2505
Mass transfer coefficient (k_m, $m s^{-1}$)		
2 $Nm^3 h^{-1}$; Re = 368	0.00232	0.00461
4 $Nm^3 h^{-1}$; Re = 736	0.00339	0.00676
6 $Nm^3 h^{-1}$; Re = 1103	0.00424	0.00844

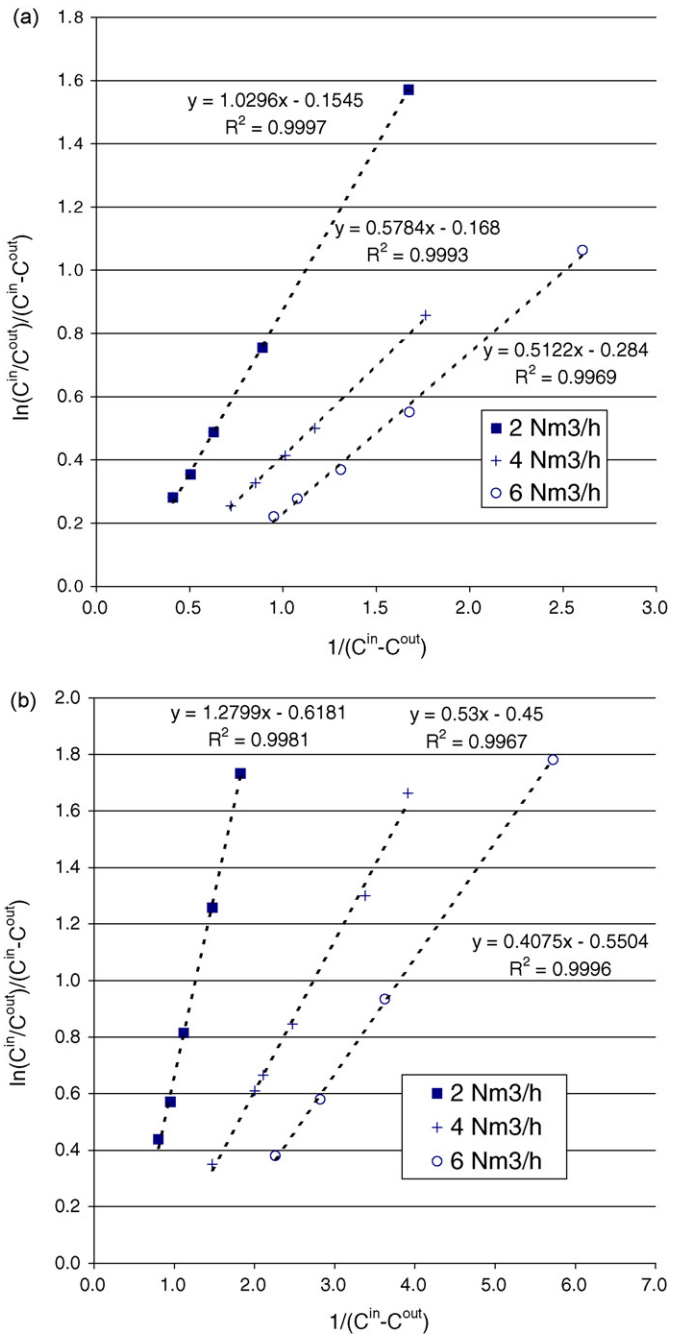

Fig. 7. Linear regression of the results with Eq. (7) for butyric acid (a) and ammonia (b) for different flow rates.

approach the solution of the non-simplified system using the series method. Furthermore it has been established that the second order development is accurate enough due to our equipment and analysis precision, as no significant differences in parameters assessment, less than 5%, were observed between second order and third order approaches [20]. The second order development of the approached solution is

$$C^{out} = C^{in} - \frac{Lk_m a_v}{2u}\left[C^{in} + \frac{1}{K} + \frac{k}{k_m a_v} - \sqrt{\left(-C^{in} + \frac{1}{K} + \frac{k}{k_m a_v}\right)^2 + \frac{4C^{in}}{K}}\right] \quad (14)$$

Table 4
Coefficients determined with the model TM

	Butyric acid	Ammonia
k (mmol m^{-3} s^{-1})	1.916	0.909
K (m^3 mmol^{-1})	0.720	0.586
R^2 (%)	99.9	99.8

The unknown parameters k and K are approximated by numerical solution using Maple. For each couple of values k and K, the least square method is applied between the experimental and theoretical outlet values. Variables for that iteration method are the L–H coefficients: k and K. The optimized coefficients with our approach are given Table 4.

First of all, correlation coefficients hold over values that underline the good predictiveness of the model MT. The determination of these parameters is realized with nonlinear regression, thus confidence interval and cross-correlation are not evaluated. This aspect has already been reported and is still in investigation [44].

With a pair of k and K values for a pollutant, that model fits the results in our whole investigated flow rate range. That model permits the separation between the mass transfer and the chemical reaction steps. As a consequence, the reaction coefficients for the L–H theory (k and K) could be considered more realistic than the ones determined with the model wMT.

The adsorption equilibrium constant K determined by the model wMT is underestimated particularly for the butyric acid; indeed with the model MT the butyric acid constant K turns out to be higher than the ammonia one. This last estimation seems to be more in accordance with the relative product volatility. The mass transfer step is less important in the ammonia case; its mass transfer coefficient k_m is twice as high as the butyric acid one. As a consequence, the difference of L–H coefficients – k and K – between both models is more significant in the butyric acid case. This aspect is also pointed out by comparing, between both models, the kK values which do not bear cross-correlation. For wMT, the kK value equals 1.38 where for MT the value is about 0.45.

The model is able to give good correlation of the experimental results of ammonia and butyric acid photooxidation, though they present dissimilar chemical degradation pathways.

Moreover that model gives the opportunity to split the global degradation rate into explicit mass transfer part and surface reaction part (controlled by UV irradiation, humidity, products, etc.). It permits to assess which step is a limit for a specific reactor design and thus to improve the global process.

5. Conclusion

An annular photoreactor, assimilated to a plug flow reactor, was used to carry out some experiments on degradation of butyric acid and ammonia. The influence of mass transfer was estimated by testing two models based on Langmuir–Hinshelwood approach. The model wMT consideration shows that the L–H constants (k and K) are flow rate dependant. So these parameters imply intrinsic effect of the mass transfer phase. When this last step is taken into account in the model (MT), the L–H constants becomes flow rate independent. The mass transfer step is estimated by empirical correlation. The MT model permits to estimate separately the contribution of the mass transfer step and chemical reaction step. Even if the chemical pathways degradation is different for Butyric acid and Ammonia, the MT model is adequate to correlate the experimental results. It is also possible to determine the concentration (C^*) near the catalyst surface.

This approach, based on mass transfer and chemical reaction steps, allows us to consider a possible wide range of applications of the model MT. This model may be a worth interesting tool to

improve reactors design, especially in applications that could technically not be carried out under high turbulences.

Acknowledgment

We thank the Ahlström Company which provided us with the photocatalytic medium and to Messrs. Biard and Videlo for their support.

References

[1] J.W. Erisman, P. Grennfelt, M. Sutton, The European perspective on nitrogen emission and deposition, Environ. Int. 29 (2003) 311–325.
[2] P. Le Cloirec, Les composés organiques volatils dans l'environnement, Lavoisier, Paris, 1998.
[3] J. Peral, X. Domènech, D.F. Ollis, Heterogeneous photocatalysis for purification, decontamination and deodorization of air, J. Chem. Technol. Biotechnol. 70 (1997) 117–140.
[4] J. Zhao, X. Yang, Photocatalytic oxidation for indoor air purification: a literature review, Build. Environ. 38 (2003) 645–654.
[5] A. Mills, S. Le Hunte, An overview of semiconductor photocatalysis, J. Photochem. Photobiol. A: Chem. 108 (1997) 1–35.
[6] M.R. Hoffmann, S.T. Martin, W. Choi, D.W. Bahnemann, Environmental applications of semiconductor photocatalysis, Chem. Rev. 95 (1995) 69–96.
[7] O. Carp, C.L. Huisman, A. Reller, Photoinduced reactivity of titanium dioxide, Progr. Solid State Chem. 32 (2004) 33–177.
[8] A.L. Linsebigler, G. Lu, J.T. Yates, Photocatalysis on TiO_2 surfaces: principles, mechanisms, and selected results, Chem. Rev. 95 (1995) 735–758.
[9] K.-H. Wang, H.-H. Tsai, Y.-H. Hsieh, The kinetics of photocatalytic degradation of trichloroethylene in gas phase over TiO_2 supported on glass bead, Appl. Catal. B: Environ. 17 (1998) 313–320.
[10] S. Yamazaki, S. Tanaka, H. Tsukamoto, Kinetic studies of oxidation of ethylene over a TiO_2 photocatalyst, J. Photochem. Photobiol. A: Chem. 121 (1999) 55–61.
[11] Y. Zhang, R. Yang, R. Zhao, A model for analyzing the performance of photocatalytic air cleaner in removing volatile organic compounds, Atmosph. Environ. 37 (2003) 3395–3399.
[12] J. Mo, Y. Zhang, R. Yang, Novel insight into VOC removal performance of photocatalytic oxidation reactors, Indoor Air 15 (2005) 291–300.
[13] C. Raillard, V. Hecquet, P. Le Cloirec, J. Legrand, Kinetic study of ketones photocatalytic oxidation in gas phase using TiO_2-containing paper: effect of water vapour, J. Photochem. Photobiol. A: Chem. 163 (2004) 425–431.
[14] P.F. Biard, A. Bouzaza, D. Wolbert, Photocatalytic degradation of two volatile fatty acids in monocomponent and multicomponent systems: Comparison between batch and annular photoreactor, Appl. Catal. B: Environ. 74 (2007) 187–196.
[15] A.A. Mobarak, H.A. Faragh, G.H. Sedahmed, Mass transfer in smooth and rough annular ducts under developing flow conditions, J. Appl. Electrochem. 27 (1997) 201–207.
[16] D. Chen, F. Li, A.K. Ray, Effect of mass transfer and catalyst layer thickness on photocatalytic reaction, AIChe J. 46 (5) (2000) 1034–1045.
[17] T.N. Obee, R.T. Brown, TiO_2 photocatalysis for indoor air applications: effects of humidity and trace contaminant levels on the oxidation rates of formaldehyde, toluene, and 1.3-butadiene, Environ. Sci. Technol. 29 (1995) 1223–1231.
[18] A. Bouzaza, C. Vallet, A. Laplanche, Photocatalytic degradation of some VOCs in the gas phase using an annular flow reactor. Determination of the contribution of mass transfer and chemical reaction steps in the photodegradation process, J. Photochem. Photobiol A: Chem. 177 (2005) 212–217.
[19] K. Mehrotra, G.S. Yablonski, A.K. Ray, Macro kinetic studies for photocatalytic degradation of benzoic acid in immobilized systems, Chemosphere 60 (2005) 1427–1436.
[20] P.F. Biard, A. Bouzaza, D. Wolbert, Photocatalytic degradation of two volatile fatty acids in an annular plug-flow reactor: kinetic modeling and contribution of mass transfer rate, Environ. Sci. Technol. 41 (2007) 2908–2914.
[21] H. Mozzanega, J.M. Herrmann, P. Pichat, NH_3 oxidation over UV-irradiated TiO_2 at room temperature, J. Phys. Chem. 83 (1979) 2251–2255.
[22] S. Yamazoe, T. Okumura, Y. Hitomi, T. Shishido, T. Tanaka, Mechanism of photo-oxidation of NH_3 over TiO_2: Fourier transform infrared study of the intermediate species, J. Phys. Chem. C. 111 (2007) 11077–11085.
[23] E.-M. Bonsen, S. Schroeter, H. Jacobs, J.A.C. Broekaert, Photocatalytic degradation of ammonia with TiO_2 as photocatalyst in the laboratory and under the use of solar radiation, Chemosphere 35 (1997) 1431–1445.
[24] J. Zhu, A review of microbiology in swine manure odor control, Agricult. Ecosyst. Environ. 78 (2000) 93–106.
[25] N. Guigand, Odeurs et environnement, cas de la production porcine, ITP, Paris, 1998.
[26] S.S. Shiffman, J.L. Benett, J.H. Raymer, Quantification of odors and odorants from swine operations in North Carolina, Agricult. Forest Meteorol. 108 (2001) 213–240.
[27] F. Benoit-Marquie, U. Wilkenhoner, V. Simon, A.M. Braun, E. Oliveros, M.T. Maurette, Voc degradation at the gas-solid interface of a TiO_2 photocatalyst. Part I. 1-butanol and 1-butylamine, J. Photochem. Photobiol. A: Chem. 132 (2000) 225–232.
[28] G.D. Lee, A. Tuan, J.L. Falconer, Photocatalytic oxidation and decomposition of acetic acid on titanium silicate, Environ. Sci. Technol. 35 (2001) 1252–1258.
[29] M.J. Backes, A.C. Lukaski, D.S. Muggli, Active sites and effects of H_2O and temperature on the Photocatalytic oxidation of ^{13}C-acetic acetic acid on TiO_2, Appl. Catal. B: Environ. 61 (2005) 21–35.
[30] C. Vallet, Dégradation photocatalytique de composés odorants en phase gazeuse—application aux effluents d'élevage porcin. Thèse de l'Université de Rennes I, 2006, p. 3358.
[31] K. Teramura, T. Tanaka, S. Yamazoe, K. Arakaki, T. Funabiki, Kinetic study of photos-SCR with NH_3 over TiO_2, Appl. Catal. B: Environ. 53 (2004) 29–36.
[32] K. Teramura, T. Tanaka, T. Funabiki, Photassisted selective catalytic reduction of NO with ammonia in the presence of oxygen over TiO_2, Langmuir 19 (2003) 1209–1214.
[33] N.W. Cant, J.R. Cole, Photocatalysis of the reaction between ammonia and nitric oxide on TiO_2 surfaces, J. Catal. 134 (1992) 317–330.
[34] S. Devahasdin, C. Fan, K. Li, D.H. Chen, TiO_2 photocatalytic oxidation of nitric oxide: transient behavior and reaction kinetics, J. Photochem. Photobiol. A: Chem. 156 (2003) 161–170.
[35] C. Vallet, A. Bouzaza, N. Prado, J. Dussaud, A. Laplanche, Photocatalytic degradation of ammonia in gas phase on batch reactor. Chemical reaction pathways and effect of the operating conditions, in: Environmental Applications of Advanced Oxidation Processes, First European Conference on Environmental Applications of Advanced Oxidation Processes, Chania, Greece, 2006.
[36] K.-P. Yu, G.W.M. Lee, W.-M. Huang, W. Chihcheng, S. Yang, The correlation between photocatalytic oxidation performance and chemical/physical properties of indoor volatile organic compounds, Atmosph. Environ. 40 (2006) 375–385.
[37] M.A. Fox, M.T. Dulay, Heterogeneous photocatalysis, Chem. Rev. 93 (1993) 341–357.
[38] A. Bouzaza, A. Laplanche, Photocatalytic degradation of toluene in the gas phase: comparative study of some TiO_2 supports, J. Photochem. Photobiol. A: Chem. 150 (2002) 207–212.
[39] D.F. Ollis, Kinetic disguises in heterogeneous photocatalysis, Topics Catal. 35 (2005) 217–223.
[40] J. Peral, D.F. Ollis, Heterogeneous photocatalytic oxidation of gas-phase organics for air purification: acetone, 1-butanol, butyraldehyde, formaldehyde and *m*-xylene oxidation, J. Catal. 136 (1992) 554–565.
[41] G. Vincent, P.M. Marquaire, O. Zahraa, Abatement of volatile organic compounds using an annular photocatalytic reactor: study of gaseous acetone, J. Photochem. Photobiol. A: Chem. 197 (2008) 177–189.
[42] P.B. Weisz, C.D. Prater, Interpretation of measurements in experimental catalysis, Adv. Catal. 6 (1954) 143–196.
[43] R.H. Perry, D. Green, J.O. Maloney, Perry's Chemical Engineers's Handbook, seventh ed., Mc-Graw Hill, New York, 1997.
[44] B. Boulinguiez, P. Le Cloirec, D. Wolbert, Revisiting the determination of Langmuir parameters—application to tetrahydrothiophene adsorption onto activated carbon, Langmuir 24 (2008) 6420–6424.